

We are IntechOpen, the world's leading publisher of Open Access books Built by scientists, for scientists

4,800

Open access books available

122,000

International authors and editors

135M

Downloads

Our authors are among the

154

Countries delivered to

TOP 1%

most cited scientists

12.2%

Contributors from top 500 universities

**WEB OF SCIENCE™**Selection of our books indexed in the Book Citation Index
in Web of Science™ Core Collection (BKCI)

Interested in publishing with us? Contact book.department@intechopen.com

Numbers displayed above are based on latest data collected.

For more information visit www.intechopen.com

Physiological Nondimensional Indices in Medical Assessment: For Quantifying Physiological Systems and Analysing Medical Tests' Data

Dhanjoo N. Ghista

*Department of Graduate and Continuing Education,
Framingham State University, Framingham, Massachusetts,
USA*

1. Introduction

1.1 Concept of Non-Dimensional Physiological Indices (NDPIs) or Physiological Numbers (PHYNs)

In this chapter, we are providing a new concept in physiological systems analysis (or organ systems analysis), in terms of nondimensional physiological indices (or physiological system numbers), for qualifying patient health and disease status as well as patient improvement.

The concept of a Nondimensional Physiological Index (or NDPI) is quite new, and has been adopted from Engineering, wherein nondimensional numbers (made up of several terms) are employed to characterize disturbance phenomena. For example, in a cardiovascular fluid-flow regime, the Reynold's number

$$N_{re} = \rho V D / \mu \quad (1)$$

is employed to characterize the conditions when N_{re} exceeds a certain critical value, at which laminar blood flow changes to turbulent flow. This can occur in the ascending aorta when either the aortic valve is stenotic (giving rise to murmurs) or in the case of anaemia (decreased blood viscosity).

In physiological medicine, the use of nondimensional indices or numbers can provide a generalized approach by which unification or integration of a number of isolated but related events into one nondimensional physiological index (NDPI) can help to characterize an abnormal state associated with a particular organ or physiological system or an anatomical structure. The evaluation of the distribution of the values of such NDPI(s), in a big patient-population, can then enable us to designate normal and disordered ranges of NDPI, with a critical value of NDPI separating these two ranges. In this way, NDPI(s) can help us to formulate patient-health indices (PHIs), not only to facilitate differential diagnosis of patients but to assess the severity of the disease or disorder as well [1,2].

This chapter is based on the author's paper: Nondimensional Indices for Medical Assasment, in *Mechanics in Medicine and Biology*, Vol 9, No 4, 2009, World Scientific Publishers.

In medicine, assessment tests are carried out to (i) determine the functional performance of an organ (such as the heart) or a physiological system (such as the glucose-insulin regulatory system), and (ii) diagnose an anatomical structure's pathological condition, such as a calcified mitral valve or osteoporosis. In many cases, the medical tests do not quantifiably assess the concerned oral or physiological system and do not quantifiably diagnose the pathological condition of the anatomical structures.

So for some conventional tests (such as the Treadmill test to assess heart function, and Oral glucose tolerance test to diagnose diabetes), we have developed NDPI (s) made up of parameters that (i) are associated with the methodology of the tests, and (ii) characterise the function and disease states of organs (such as the heart) and physiological systems (such as the glucose-insulin regulatory system). We have also developed some new medical tests to detect anatomical structures' pathology (such as arteriosclerosis and mitral valve calcification) in terms of NDPI (s) to characterize their pathological state. In this chapter, we have formulated nine medical tests and their associated NDPI (s).

We would like that the NDPI (s) developed in this chapter, for both conventional tests as well as newly formulated tests, can be applied clinically to set the stage for more accurate medical assessment. These medical tests and their associated NDPI (s) need to be applied to large patient population, to determine the normal and abnormal (or pathological) ranges of these NDPI (s). This will enable incorporation of our newly formulated NDPI (s) into medical practice.

2. Cardiac contractility index

Let us provide an example of one of our NDPI(s) which has been clinically employed. In cardiology, the index $(dP/dt)_{max}$ (of maximum rate-of-increase of left ventricular chamber pressure) has been traditionally employed as a measure of cardiac contractility. Diminished cardiac contractility affects cardiac output and can lead to heart failure. Hence, this is an important index of left ventricle (LV) functional capability. However, this index requires the invasive measurement of LV chamber pressure by catheterization. So, we developed an alternative cardiac contractibility index in terms of the normalised wall stress of the LV with respect to LV chamber pressure, $\sigma^* = \sigma / P$. Now, corresponding to $(dP/dt)_{max}$, we have formulated the cardiac contractility index (CCI) of $d\sigma^*/dt_{max}$, which does not require the measurement of LV chamber pressure. This contractility index can be conveniently expressed in terms of LV chamber cavity volume (V) and myocardial volume (V_m), as indicated in Ref 4. as well as in this section 5 of chapter 34 on how cardiac disease states cause decreased contractility and how surgical ventricular restoration improves contractility. By employing a thick-walled spherical LV model with inner and outer radii r_i and r_e , we can express LV pressure-normalised wall stress (σ^*) as [3,4]:

$$\sigma^*(r = r_i) = \left(\frac{3V}{2V_m} + \frac{1}{2} \right) \quad (2)$$

where $V(=4\pi r_i^3/3)$ denotes LV volume, and $V_m(=4\pi(r_e^3-r_i^3)/3)$ denotes LV myocardial volume. Then by differentiating σ^* with respect to time, we get the expression for CCI as:

$$CCI, d\sigma^*/dt_{max} = \left. \frac{d(\sigma_\theta/p)}{dt} \right|_{max} = \frac{3}{2V_m} \left. \left(\frac{dV}{dt} \right) \right|_{max} \quad (3a)$$

At the National Heart Center (in Singapore General Hospital), we have validated $d\sigma^*/dt_{max}$ against dP/dt_{max} in subjects with disparate ventricular function (as illustrated by figure 6 in chapter 34) and demonstrated the index's load independence. For normal subjects, this index value range is 4 - 4.5 s⁻¹. We have also successfully employed this $(d\sigma^*/dt)_{max}$ contractility index to assess (i) reduced LV contractility in ischemic cardiomyopathy patients in the range of $2.64 \pm 0.74s^{-1}$ and (ii) improved contractility in the range of $3.32 \pm 0.73 s^{-1}$ following surgical ventricular restoration [5].

We could even divide this CCI index by the heart rate, and make it nondimensional, as:

$$CCI-2 = (100) [d\sigma^* / dt_{max}] / HR \left(ins^{-1} \right) \quad (3b)$$

For normal hearts (with HR in the range of 60-80 per min), this index would give values in the range of 300-500, while for ischemic cardiomyopathic hearts (and HR greater than 100 per min) this index would be in the range of 200 and below. This CCI-2 index would even more reliably represent cardiac contractility, by more distinctly differentiating ischemic and infarcted hearts from normal hearts.

3. Assessing cardiac fitness and heart function

In this section, we show how the conventional Treadmill test can be formulated in biomedical engineering terms, to derive a cardiac fitness index to detect a malfunctioning heart due to, for instance, an infarcted heart caused by coronary occlusion.

The Treadmill test's cardiac fitness model consists of a first-order differential-equation system models, describing the heart rate (HR) response (y) to exertion (exercise, jogging, etc.) monitored in terms of a constant work-load or power (W), where y is defined as follows [6,2]

$$y = \frac{HR(t) - HR(rest)}{HR(rest)} \quad (4)$$

In a Treadmill test, the subject is asked to exercise on the treadmill for a period of time, t_e (min). During this period, the $HR(t)$ (and hence y) is monitored. Now we develop a model to simulate (i) the $HR(t)$ response to during exercise, i.e. $t < t_e$ and (ii) thereafter for $HR(t)$ decay after the termination of exercise (as illustrated in figure 1).

The DEq for y response to exercise on the treadmill at a constant work-load or power exerted (W) is given by

$$\begin{aligned} \frac{dy}{dt} + k_1 y &= C_0 W, \text{ for } t \leq t_e \\ \frac{dy}{dt} + k_2 y &= 0, \text{ for } t \geq t_e \end{aligned} \quad (5)$$

where (1) k_1 and k_2 are the model parameters, and (2) C_0 is a conversion factor to express W in the same units as the other terms of the equation. The y solutions to equations (5) are represented by:

$$y = \frac{C_0 W}{k_1} (1 - e^{-k_1 t}), \text{ for } t \leq t_e \text{ during the exercise} = \frac{y_e (1 - e^{-k_1 t})}{(1 - e^{-k_1 t_e})} \quad (6)$$

$$y = y_e e^{-k_2(t-t_e)}, \text{ for } t \geq t_e \text{ during the recovery period when } W=0 \quad (7)$$

where $y_e = y(t=t_e)$, and k_1 and k_2 are the model parameters which can serve as cardiac fitness parameters (in units of min^{-1}).

We now carry out parametric simulation to the monitored HR data on treadmill, by making equations (6 and 7) fit the HR data. The parameters k_1 and k_2 can be combined into a non-dimensional fitness index CFI given by:

$$CFI = k_1 k_2 t_e^2 \quad (8)$$

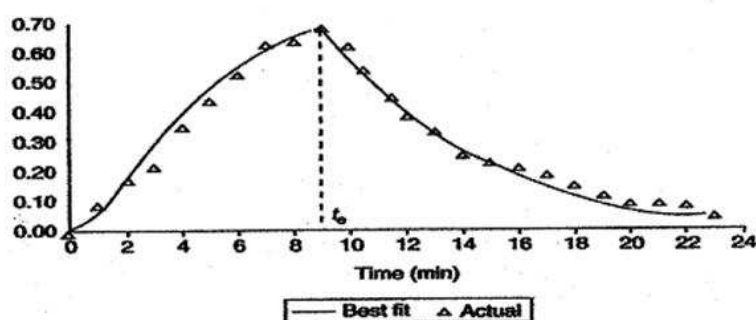


Fig. 1. Sample subject's monitored y versus t data (Adopted from Ref 6: Lim GeokHian, Dhanjoo N. Ghista, Koo TseYoong, John Tan Cher Chat, Philip EngTiew & Loo Chian Min; *International Journal of Computer Application in Technology: Biomedical Engineering & Computing Special Issue*, Vol 21, No 1/2, 2004.).

According to this formulation of CFI , for subjects exercised at identical workloads, a healthier subjects would have (1) greater k_1 (i.e., slower rate of increase of HR during exercise), (2) greater k_2 (i.e., faster rate of decrease of HR following exercise), (3) greater t_e (i.e., exercise endurance); and hence (4) higher value of CFI .

We need to evaluate CFI for a big spectrum of patients, and then compute its distribution curve, to determine the efficacy of this index, in order to yield distinct separation of CFI ranges for healthy subjects and cardiac patients. This CFI can then also be employed to assess improvement in cardiac fitness following cardiac rehabilitation regime.

4. Lung ventilation Index to detect lung disorders

Herein, we are formulating a new test involving: (i) monitoring of lung volume by means of a spirometer; (ii) the biomedical engineering model of the lung volume response to lung inflation driving pressure, which is equal to mouth pressure minus pleural pressure monitored by placing a balloon catheter transducer through the nose into the esophagus; (iii) derivation of the lung ventilation index made up of the parameters of the lung volume response model, and its employment to detect lung disorders.

The differential equation of lung ventilation volume (V) response to lung inflation-pressure (P_I) is given (as illustrated in figure 2) by [1, 2]:

$$\begin{aligned} R \frac{dV}{dt} + \frac{V}{C} &= P_D = (P_0 - P_p) - \left(P_p @ \text{end-expiration} \right) \\ &= P_1 - P_1 \cos \omega t + P_2 \cos \omega t \end{aligned} \quad (9)$$

wherein V is the lung volume in litres (L), P_0 is the pressure at the mouth (in cm H₂O) and P_p is the pleural pressure (in cm H₂O). The right-hand side terms constitute the Fourier series representation of the lung driving pressure (P_D) in cm H₂O, R is the resistance to airflow (in cm H₂O · S · L⁻¹), C is the lung compliance (in L/cm H₂O), and P_1 and P_2 are the magnitudes of Fourier series terms of the lung driving (oscillatory) pressure P_D [= (mouth-pressure minus pleural-pressure), with respect to the absolute value of end-expiratory pleural pressure]. For a typical P_D cyclic pressure profile (Fig.2), represented by

$$P_1 = 1.84 \text{ cm H}_2\text{O}, \quad P_2 = 3.16 \text{ cm H}_2\text{O}, \quad \omega = 0.5\pi \text{ s}^{-1},$$

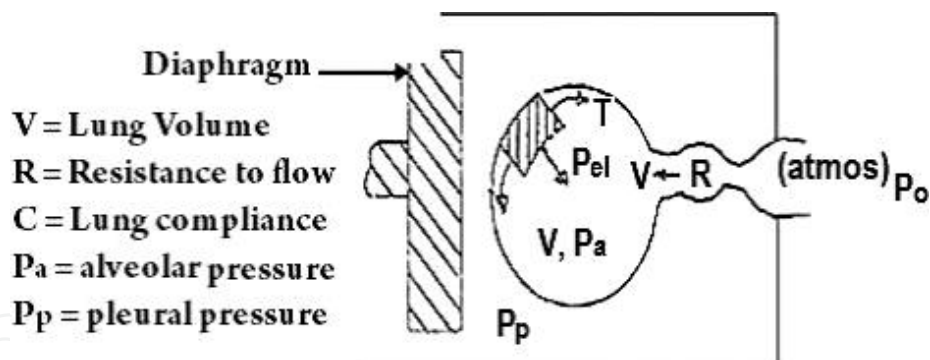
the solution to the above Eq. (9) is given by

$$V = P_1 C \left(1 - e^{-t/\tau}\right) - P_1 C \frac{(\cos \omega t + \omega \tau \sin \omega t)}{1 + \omega^2 \tau^2} + P_2 C \frac{(\sin \omega t + \omega \tau \cos \omega t)}{1 + \omega^2 \tau^2} + \frac{e^{-t/\tau}}{(1 + \omega^2 \tau^2)} \left[P_1 C (1 + 2\omega^2 \tau^2) + P_2 C (\omega \tau) \right] \quad (10)$$

wherein $\tau = RC$. By fitting this lung volume solution to the clinically monitored lung-volume parameters, we get: $R = 1.24 \text{ (cm H}_2\text{O) sL}^{-1}$, $C = 0.21 \text{ L (cm H}_2\text{O)}^{-1}$. Now, then, let us formulate the nondimensional lung ventilator performance index (LVPI-1) given by:

$$\text{LVPI-1} = RC \text{ (BR per min)}, \quad (11)$$

wherein BR, the breathing rate = $30\omega/\pi$ per min = 15/min or 0.25/sec for the data provided in Fig.2. For our case study, the value of LVPI is 3.9.



$$\begin{aligned} P_L &= P_o - P_p \\ &= (P_o - P_a) + (P_a - P_p) = (P_o - P_a) + P_{el} \\ &= \left(R \frac{dV}{dt} \right) + \left(\frac{V}{C} + P_{el} @ t = T \right) \\ &= \left(R \frac{dV}{dt} \right) + \left(\frac{V}{C} - P_p @ t = T \right) \end{aligned}$$

$$\text{Driving Pressure, } P_D = P_L - \left| P_p @ t = T \right|$$

Fig. 2. Lung Ventilation Lumped parameter model.

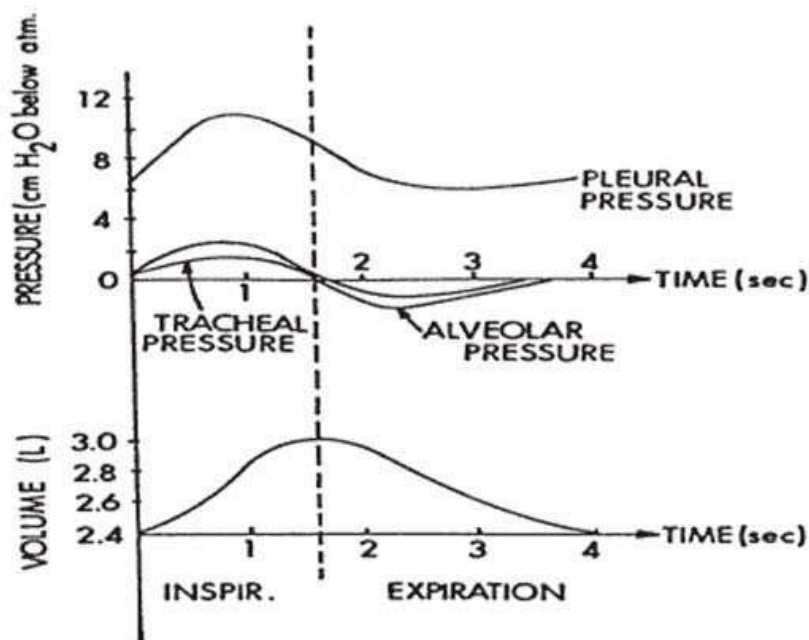


Fig. 3. Lung pressure and volume as functions for normal breathing; note that the pressure extremes occur before the volume extremes.

Let us now see how lung disease will influence R , C and hence $LVPI$. For instance in emphysema, the destruction of lung tissue will produce a more compliant lung and hence a larger value of $C = 0.5L (cm H_2O)^{-1}$, say, yielding a value of $LVPI$ of about 10. In asthma, there is increased airway resistance (due to contraction of the smooth muscles around the airways) to say $R=5(cm H_2O) sL^{-1}$. The breathing rate can also go up to $BR = 20/min$, say. Hence, the value of $LVPI$ can go up to 20. In the case of lung-congestion, due to mitral-valve disease, it would be important to determine $LVPI$, so as to serve as an indicator for determining cardiac condition (in end-stage heart-disease). By determining the distribution of a big patient population, we can determine the $LVPI$ ranges for normal and disease states.

Now this procedure refers to monitoring of pleural pressure (P_p) by placing a balloon catheter transducer through the nose into the esophagus (assuming that the esophageal tube pressure equals the pressure in the pleural space surrounding it). So, let us now develop a procedure whereby we do not need to monitor pleural pressure and only need to monitor lung volume by means of a spirometer. For this purpose, we now identify three model parameters (P_1C), (P_2C) and τ . These parameters can be determined by having equation (10) match or simulate the lung volume data in figure 3. We now formulate a non-invasively determinable nondimensional ventilator index ($LVPI-2$), as

$$LVPI-2 = \frac{(BR)\tau(TV)^2}{(P_1C)(P_2C)}, \quad TV = \text{tidal volume} \quad (12)$$

Upon evaluating $LVPI-2$ for a number of patients, we can determine its ranges for normal and disease states, to employ it diagnostically. We can expect that subjects with chronic obstructive lung disease (COPD) and asthma subjects (with a high value of R) will have a high value of $LVPI-2$, while emphysema subjects (with high value of C) will have a low value of $LVPI-2$. So in the distribution curve of $LVPI-2$, emphysema subjects will be at the

low end of distribution curve, COPD and asthma subjects will be at the high end of the distribution curve, while normal subjects will be in the middle of the distribution curve.

Now for noninvasive assessment of lung disease state in terms of lung compliance (C) and resistance-to-flow (R), we need to be able to determine lung pressure (P_D) function noninvasively. In section 4 of chapter 36 on lung ventilation modeling for assessment of lung station we have shown how we can determine the lung driving pressure functional parameters along with C and R in terms of the monitored values of lung volume.

We have also formulated a non-dimensional lung ventilatory index (equation 30) in terms of R, C, tidal volume (TV), lung pressure value at TV and breathing rate. After this index is evaluated for different disease states, it will enable reliable noninvasive assessment of lung status.

5. Diabetes diagnosis from oral-glucose-tolerance test by means of a diabetes index (OGTT)

In this section, we have developed a biomedical engineering model for OGTT and demonstrated how it can be applied to OGTT data in (figure 4) to formulate and evaluate a diabetic NDPI, to more reliably diagnose diabetes.

For oral-glucose tolerance test simulation (entailing digestive and blood-pool chambers), the differential equation, and governing blood-glucose response (y) to oral ingestion of glucose bolus (G , gm L⁻¹hr⁻¹), given by[7]:

$$y'' + 2Ay' + \omega_n^2 y = G\delta(t); y \text{ in gL}^{-1}, G \text{ in gL}^{-1}\text{hr}^{-1}$$

$$y'' + \lambda T_d y' + \lambda y = G\delta(t) \tag{13}$$

where $\omega_n (= \lambda^{1/2})$ is the natural oscillation-frequency of the system, A is the attenuation or damping constant of the system, $\omega = (\omega_n^2 - A^2)^{1/2}$ is the (angular) frequency of damped oscillation of the system, $\lambda (2A/T_d = \omega_n^2)$ is the parameter representing regulation proportional to rate-of-change of glucose concentration (y), and λT_d is the parameter representing regulation proportional to rate-of-change of glucose concentration (y').

Figure 4 illustrates the OGTT data for typical normal and diabetic subjects. For an impulse glucose ingestion input, we can simulate a normal patient's blood-glucose concentration data by means of the solution of the Oral glucoseregulatory (second-order system) model, as an under-damped glucose-concentration response curve, given by:

$$y(t) = \left(\frac{G}{\omega}\right) e^{-At} \sin \omega t, \tag{14}$$

When this solution is made to simulate the normal subjects OGTT data, we get $A=1.4 \text{ hr}^{-1}$, $\omega = 0.775 \text{ rad/hr}$, $G = 1.04 \text{ gL}^{-1} \text{ hr}^{-1}$, $\lambda = 2.6 \text{ hr}^{-2}$, $T_d = 1.08 \text{ hr}$. The simulated curve is also depicted in figure 4.

For a potential diabetic subject, we adopt the solution of the above Differential equation model, as an over-damped response function:

$$y(t) = \left(\frac{B}{\omega}\right) e^{-At} \sinh \omega t. \tag{15}$$

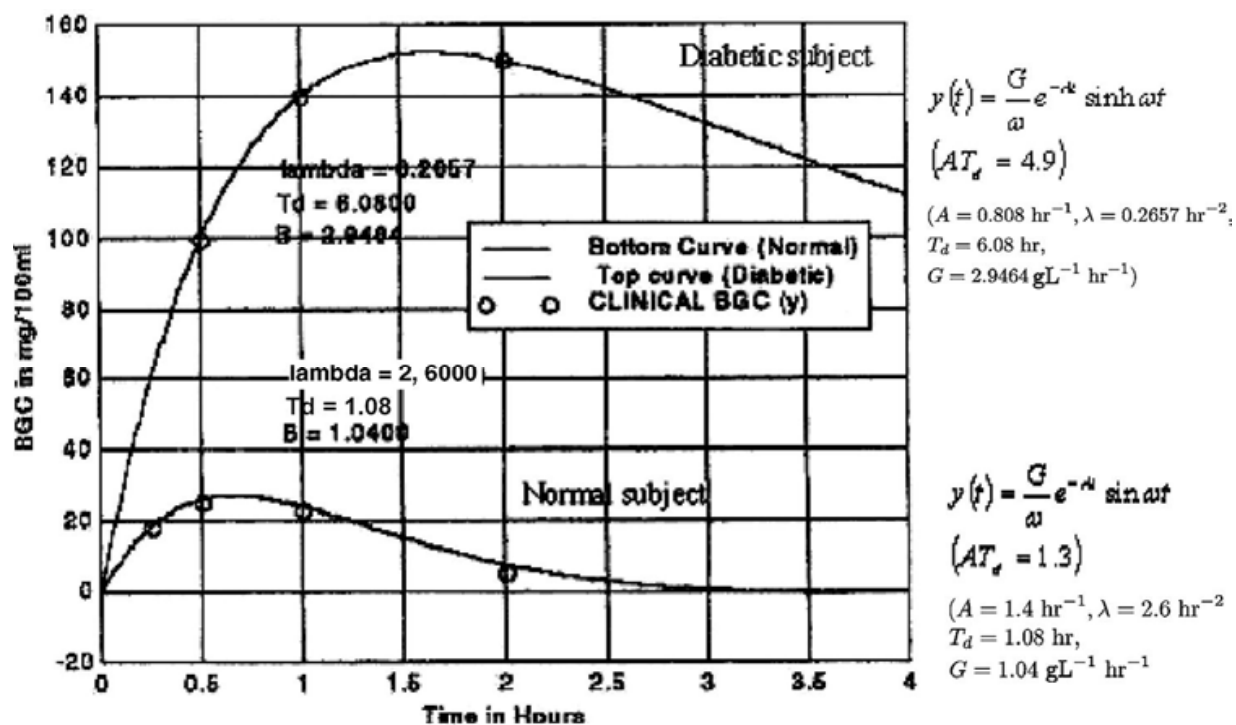


Fig. 4. OGTT Response Curves: $A = 1.4 \text{ hr}^{-1}$ (i.e. higher damping-coefficient value) for the normal subject for the diabetic patient, $A = 0.808 \text{ hr}^{-1}$. Also, for the normal subject, the regulation parameters λ and λT_d are 2.6 hr^{-2} and 2.8 hr^{-1} respectively, which are greater than their values of 0.26 hr^{-2} and 1.62 hr^{-1} for the diabetic subject. Further, the non-dimensional number for the normal subject is 1.3, compared to 4.9 for the diabetic subject.

For this OGTT data simulated function (figure 4), the parameters values are: $A = 0.808 \text{ hr}^{-1}$, $\omega = 0.622 \text{ rad hr}^{-1}$, $G = 2.95 \text{ gL}^{-1} \text{ hr}^{-1}$, $\lambda = 0.266 \text{ hr}^{-2}$, $T_d = 6.08 \text{ hr}$.

Now, we come to the interesting part of this model, by formulating the nondimensional Diabetes index (*DBI*) as:

$$DBI = AT_d = \frac{2A^2}{\lambda} = \frac{2A^2}{\omega_n^2}. \quad (16)$$

The value of *DBI* for the normal subject is found to be 1.5, whereas that for the diabetic subject is 4.9. It is further seen (in our initial clinical tests) that *DBI* for normal subjects is < 1.6 , while the *DBI* for diabetic patients is > 4.5 . This is a testimony of the efficacy of the model, and especially for the nondimensional *DBI*.

Now between these two cases of under-damped and over-damped responses, we have the case of a critically-damped response, for which the solution of the OGTT model differential equation (13) is given by

$$y(t) = Gte^{-At}, \text{ for which } \omega = 0, \text{ and } A^2 = \lambda = \omega_n^2$$

This critically-damped response corresponds to cases of subjects who are not distinctly normal or diabetic but are at the risk of becoming diabetic. It can be seen that *DBI* for the critically-damped response is 2. So, in the distribution curve of *DBI* (to be obtained by applying this method to a large patient population), the *DBI* range of less than 1.6 would

refer to normal subjects, the range of greater than 4.5 would refer to diabetic subjects, and range of 2-4 would refer to subjects at risk of becoming diabetic. This would make the use of the model and the *DBI* to be so convenient for the physician.

6. Characterization of arterial stiffness or arteriosclerosis by means of NDI

In this section, we are formulating a new test to noninvasively determine the arterial constitutive property so as to be able to diagnose arteriosclerosis. For a circular cylindrical arterial tube of radius *a* and wall-thickness *h*, we can express the stress σ and elastic-modulus *E*, as follows:

$$\sigma = \frac{Pa}{h} = \frac{130Pa}{h} N / m^2; E = \frac{2(PWV)^2 a\rho}{h}; E = E_0 + m\sigma \tag{17}$$

in terms of (i) the arterial dimensions *a* and *h*, the auscultatory (or automatedly) measurable diastolic pressure (*P*) and pulse-wave velocity (*PWV*) determined by ultrasound [8]. The table below then depicts the computed values of σ and *E* at four independent times.

<i>P</i> (mmHg)	<i>PMV</i> (m/s)	<i>A</i> (mm)	<i>h</i> (mm)	$E \left[\frac{N}{m^2} \right]$	$\sigma \left[\frac{N}{m^2} \right]$
80	5.3	4.1	1.10	2.13×10^5	3.38×10^4
85	5.4	4.5	1	2.6×10^5	4.97×10^4
90	5.42	5.0	0.90	3.01×10^5	5.97×10^4
95	5.5	5.0	0.90	3.38×10^5	6.68×10^4

Table 1.

$$\text{Result: } E \left(N/m^2 \right) = 4.2\sigma + 0.5 \times 10^5 \left(N/m^2 \right) = m\sigma + E_0. \tag{18}$$

We will now define the arteriosclerotic non-dimensional index

$$ART - NDI = mE_0 / (\text{mean diastolic pressure}) \tag{19}$$

For the above patient, the value of the *ART - NDI* is

$$ART - NDI = \frac{(4.2)(0.5 \times 10^5 N/m^2)}{(87 \times 137 N/m^2)} = 17.6 \tag{20}$$

and will be much higher for arteriosclerotic patients, which we will determine by conducting clinical tests-applications of this analysis. This *ART-NDI* to detect arteriosclerosis requires echocardiographic determination of arterial dimensions and *PWV*[8], and auscultatory diastolic pressure.

7. To non-invasively determine aortic elasticity (m), peripheral resistance (R), aortic NDI, and aortic pressure profile

Herein, we have developed the analysis to noninvasively determine the aortic pressure profile, which can have significant diagnostic applications. This analysis is also employed to

determine (i) aortic volume elasticity parameter m ($=dP/dV$), (ii) peripheral resistance parameters $R=P(\text{pressure})/Q(\text{flow rate})$, and (iii) the aortic property NDPI, given by aortic number. Based on the aorta fluid mechanics model (figure 5), we obtain:

$$\frac{dV}{dt} = I(t) - Q(t) = I(t) - P(t) / R \quad (21-a)$$

$$\frac{dP}{dt} = \frac{dP}{dV} \frac{dV}{dt} = m \frac{dV}{dt} \quad (21-b)$$

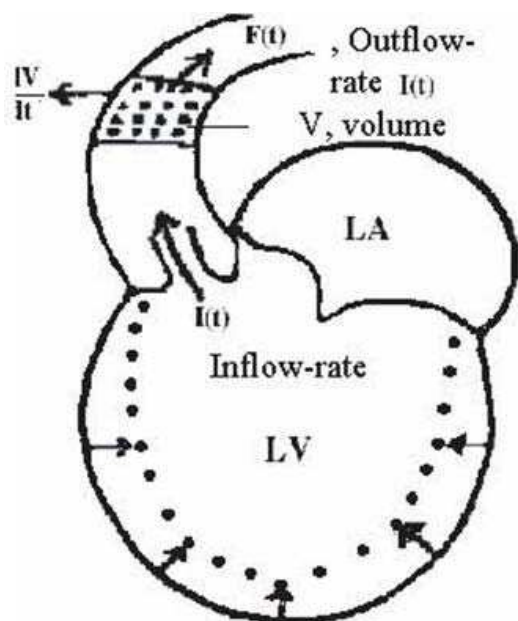
We can then put down the aortic pressure (P) response to aortic inflow-rate or LV outflow-rate $I(t)$ as follows [9,1] :

$$\frac{dP}{dt} + \lambda P = mI(t); \quad (22)$$

wherein, m = Volume elasticity of aorta (in Pa/m³), and $\lambda = (m/R)$ in s⁻¹.

The LV outflow-rate is represented as:

$$I(t) = (A) \sin(\pi / t_s) t + (A / 2) \sin(2\pi / t_s) t, \quad 0 < t < t_s \text{ (systole)} \\ = 0; \quad t > t_s \text{ (diastole)} \quad (23)$$



Aortic pressure, $P(t)$
 TPR, $R(t)$
 Aortic (volume) elasticity, m
 $\lambda = m/R$

Given:

$$I(t) = (A) \sin(\pi/t_s) t + (A/2) \sin(2\pi/t_s) t, \quad 0 < t < t_s \\ = 0, \quad t > t_s$$

$$T_s = 0.35s, \quad SV = 71.4 \text{ cc}$$

$$A = 320 \text{ cc/s}$$

$$\frac{dV}{dt} = I(t) - F(t) = I(t) - \frac{P(t)}{R}, \quad \frac{dP}{dt} = -\left(\frac{m}{R}\right)P + mI(t) \\ \therefore (dP/dt) + \lambda P = mI(t)$$

Fig. 5. To derive the equation for Aortic-pressure response to the stroke-volume or LV output rate $I(t)$.

If $t_s = 0.35s$, and Stroke vol(SV) is known (from, say, echocardiography), then we have

$$\int_0^{t_s} [(A) \sin(\pi/t_s) t + (A/2) \sin(2\pi/t_s) t] dt = SV \quad (24)$$

wherein $A = \pi(SV) / 2t_s$

$$\text{So if } SV = 71.4cc, \text{ then } A = 320cc/s. \quad (25)$$

The solutions of Eq. (22) for the aortic diastolic and systolic periods are obtained as follows [9,1]:

Aortic Diastolic Pressure expression (fig 6):

$$\begin{aligned} P_d(t) &= P_2 e^{-\lambda(t-t_s)}; \quad P_2 = \text{pressure at start of diastole} \\ &= P_1 \text{ (at } t = T) = \text{pressure at end of systolic phase} \\ \therefore P_d(t) &= P_1 e^{\lambda(T-t)}, \quad \text{wherein } T = 0.8s. \end{aligned} \quad (26)$$

This $P_d(t)$ function is equal to P_2 at $t = t_s$ (at the end of systolic phase) and P_1 at $t = T$ (end of diastolic phase).

Aortic Systolic Pressure expression (fig 6):

$$\begin{aligned} P_s(t) &= \left(P_1 + \frac{Am\omega}{\lambda^2 + \omega^2} + \frac{2Am\omega}{\lambda^2 + 4\omega^2} \right) e^{-\lambda t} + mA \left(\frac{\lambda \sin \omega t - \omega \cos \omega t}{\lambda^2 + \omega^2} \right) \\ &+ \frac{mA}{2} \left(\frac{\lambda \sin 2\omega t - 2\omega \cos 2\omega t}{\lambda^2 + 4\omega^2} \right); \quad \omega = \frac{\pi}{t_s}. \end{aligned} \quad (27)$$

This $P_s(t)$ function is maximum at $t = t_m$, and equal to the monitored systolic auscultatory pressure $P_3 = 118\text{mmHg}$.

We now (i) incorporate into Eqs. (26) and (27) the auscultatory data of $P_1(80\text{mmHg})$ and $P_3(118\text{mmHg})$ with $T = 0.8$ s, and $t_s = 0.35$ s, as well as (ii) invoke continuity in diastolic and systolic pressure expressions, to (iii) put down and solve the following three equations (in three unknowns: m , λ and t_m which $P_s = P_2$):

$$P_d(\text{at } t_s = 0.35s) = P_s(\text{at } t_s = 0.35s) \quad (28)$$

$$\frac{dP_s(\text{at } t_m)}{dt} = 0 \quad (29)$$

$$P_s(t = t_m) = P_3 (= 118\text{mmHg}) \quad (30)$$

to obtain: $\lambda = 0.66 \text{ s}^{-1}$, $m = 0.78 \text{ mmHg cm}^{-3}$, $R = 1.18\text{mmHg cm}^{-3} \text{ s}$, $t_m = 0.25$ s, for $T = 0.8$ s.

We now formulate the Aortic number (or index):

$$\text{Aortic number} = \lambda T = mT/R \quad (31)$$

wherein $\lambda = m/R$ in the governing differential equation (22), $m = 103 \times 10^6 \text{ Pa m}^{-3}$, $R = 157 \times 10^6 \text{ Pa m}^{-3} \text{ s}$, and $\lambda = 0.66 \text{ s}^{-1}$

$$\text{We thereby obtain the } \text{Aortic Number} = \lambda T = (0.66 \text{ s}^{-1})(0.8 \text{ s}) = 0.52. \quad (32)$$

In order to have a more convenient order-of-magnitude value of the Aortic number index (equation 31), we could employ the *Aortic number* = 100 (λT). In the distribution of *Aortic*

number (obtained by applying this methodology to a large patient population), the low range of Aortic Number will correspond to patients with vasoconstriction, the high range of Aortic Number will be associated with arteriosclerotic patients, and patients with normal healthy aorta will be in the middle of the distribution.

Finally with the help of the evaluated parameters m and R , we can now construct the aortic pressure profile based on equations (26 and 27), as illustrated in figure 6. This aortic pressure profile can have significant diagnostic implications. As we know, in Ayurvedic medicine and Chinese Traditional medicine, the physician feels the pulsation of the patients brachial artery (just proximal to the wrist), and based on it provides diagnosis of a wide spectrum of diseases. Essentially, the physician is feeling the magnitude and shape of the arterial pressure pulse.

Now, we have shown that we can in fact noninvasively determine the aortic pressure profile, which is more diagnostically indicative than the pressure pulse in the more distally located brachial artery. Hence, we can bring to bear this medical inferential and experiential knowledge to firstly characterise the magnitude and shape of the aortic pressure profile (by Fourier analysis), and then correlate the Fourier series parameters to the information about the associated disease states available from Ayurvedic and Chinese medicine systems.

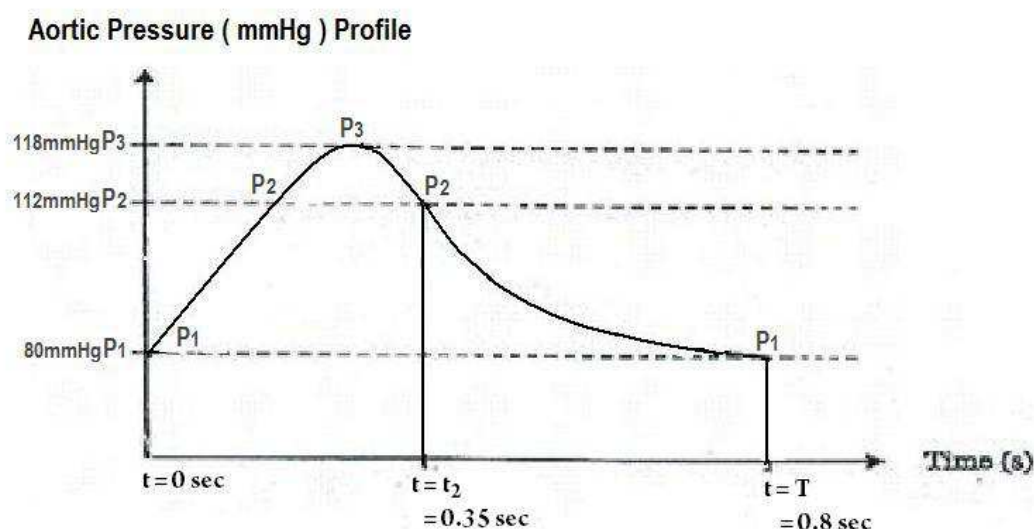


Fig. 6. Illustration of the Aortic pressure profile, based on the analysis. The systolic phase is from $t = 0$ to $t = t_s = 0.35s$. The diastolic phase is from $t = t_s = 0.35s$ to $t = T = 0.8s$.

8. Mitral-Valve (MV) property determination for its pathology characterization (to provide interventional guidelines)

Determining the in-vivo constitutive property of the mitral valve (for a quantifiable estimate of its calcification and degeneration) constitutes another example combining “clinical-data monitoring and processing” with “modelling-for-clinical diagnosis”.

The mitral valve opens at the start of the diastolic phase when the blood from the left atrium fills the left ventricle (LV). At the end of the diastolic phase and at the initiation of LV contraction phase, the rising LV pressure and the blood flow pattern in the LV chamber brings the valve cusps together to close the MV, and set its cusps into vibratory motion, which is monitored as the First Heart sound (FHS).

From a biomedical engineering consideration, the mitral valve in its closed position (at the end of the diastolic phase) can be modelled as a semi-circular membrane, which is fixed along its circular edge to the heart chamber wall and supported along its straight edge by the chordae tendineae (as depicted in figure 7), so that its deflection is zero along its edges [10,11]. In this configuration, the MV vibrates after its cusps come together to close the valve. The frequency of MV vibration (f_{mv}) (as obtained from the FHS frequency spectrum) can be expressed in terms of the MV constitutive parameter property (E vs σ), which conveys information about its health state and pathology. This methodology provide a more reliable and quantitative approach for detecting a pathological MV (such as owing to its leaflets calcification) than by merely listening to the First Heart sound (as practised clinically).

To this end, we provide the expressions for determining MV stress (σ) and its elastic modulus (E) from the physiological data of the MV vibration its closed configuration. We then develop expressions for mitral valves modulus-based property E^* and stress-based property σ^* , and propose that the E^* vs σ^* relationship be employed to characterise mitral valve pathology. Alternatively, we can also track mitral valve pathological deterioration, by monitoring the changes in valve of $m (= E/\sigma)$ in terms of the changes in f_{mv} as the valve pathology progresses, and determine the time for intervention of replacing the pathological MV by means of a prosthetic MV.

We make use of:

- echocardiography (to determine the mitra-valve geometry) and spectral phonocardiography (of the first-heart sound associated with MV vibration), to determine the second-peak frequency (f_2) of the first heart-sound spectrum
- along with static and dynamic (vibration) analyses of the semi-circular mitral valve leaflet model (held along its circular boundary), as illustrated in Fig. 7, to obtain the following expressions [10 & 11], for

$$\text{Stress } (\sigma) \text{ in the leaflet membrane} = \frac{\pi_2 f_2^2 a^2 \rho}{(K_{nm} / 2)^2}, \quad (33)$$

wherein a is the radius of the semi-circular leaflet; ρ is the leaflet membrane density per unit area; K_{nm} is the m th zero of the n th order Bessel function $J_n(k)$, m (number of nodal circles) = 1, and (number of nodal diameters)=1, and $k_{11} = 3.832$.



Fig. 7. The mechanism of MV closure and subsequent vibration, in the genesis of the first-heart sound. Functional mechanics of the Mitral valve: (a) mitral valve opening at start of left centricular diastole; (b) as the filling left ventricle distends, traction is applied through the chordae tendineae to the valve cusps, pulling them together; (c) at the start of LV systole, the valve cusps are sealed together by the high internal pressure and the flow pattern in the ventricular chamber. It is at this point in time that the mitral valve starts vibrating.

$$\text{Modulus (E) of the leaflet membrane} = \frac{\pi^8 f_2^2 \rho^3 t^2 a^4 (1-\nu)}{(K_{11}/2)^6 q_0^2 S_n}, \quad (34)$$

Wherein t = leaflet thickness, ν is the Poisson's ratio, q_0 is the pressure difference across the leaflet at time of occurrence of the closed Mitral-valve (MV) Vibration, and S_n (the summation of a series) = 0.105.

Based on eqs. (33) and (34), the nondimensional constitutive parameter (m) of the MV, is given by

$$m = \frac{E}{\sigma} = \frac{3\pi^6 f_2^4 \rho^2 t^2 a^2 (1-\nu)}{q_0^2 S_n (K_{11}/2)^4} \quad (35)$$

As a matter of interest, for the data: $f_2 = f_{mv} = 100\text{Hz}$, $q_0 = 2 \text{ mm Hg}$, $\rho = 1.02 \text{ gm/cm}^3$, $a = 1 \text{ cm}$, $t = 0.5 \text{ mm}$, $\nu = 0.5$, and evaluating S_n ($= 0.0234$, Eq 2.16, Ref.2), we get $\sigma = 2.75 \times 10^3 \text{ N/m}^2$ and $E = 1.6 \times 10^5 \text{ N/m}^2$.

Now, changes in MV pathology will affect its density (ρ) and thickness (t), as well as its modulus (E) vs stress (σ) property which we want to determine by combining FHS power-spectrum analysis (to determine f_{mv}) and 2-d echocardiographic analysis (to determine the size parameter a).

We now designate a new stress-based property (σ^*) of MV (from equation 33), as

$$\sigma^* = \frac{\sigma}{\rho} = \frac{\pi^2 f_{mv}^2 a^2}{(1.916)^2} \quad (36)$$

as well as a new modulus -based property (E^*) of MV (from equation 34), as

$$E^* = \frac{E q_0^2}{\rho^3 t^2} = \frac{\pi^8 f_{mv}^6 a^4 (1-\nu)}{(1.916)^2 S_n}, \quad (37)$$

We can now employ this E^* vs. σ^* relationship as a constitutive property of MV, to characterize and track its degeneration for timely intervention purpose.

This technology and methodology can provide the basis for timely surgical and/ or replacement intervention for a diseased MV. In order to apply this analysis, we can determine the valvular leaflet size parameter (a) from 2-D echocardiograms. The valvular leaflet vibrational frequency (f_{mv}) can be obtained from the frequency spectra of the FHS phonocardiographic signal associated with MV movement.

We can study a number of patients and determine the in vivo (E^*, σ^*) values of their valves, at a regular intervals during their degeneration process. We can also simultaneously and regularly monitor cardiac symptoms and chamber sizes and correlate them with the valcular constitutive E^* - σ^* property. By means of these correlations, we can determine the critical (E^* - σ^*) boundary at which intervention will have to be made to replace the degenerated natural valve by means of a prosthetic flexible leaflet MV.

In an alternative somewhat simpler approach, the mitral valve constitutive property parameter m (equation 35) can be employed diagnostically to track the deterioration due to calcification of the MV, in terms of Δm according to the relationship:

$$\Delta m = (\partial m / \partial f_{mn}) \Delta f_{mn} + (\partial m / \partial q_0) \Delta q_0; \text{ where in } f_{mv} = f_2 \quad (38)$$

$$\text{so that: } \frac{\Delta m}{m} = 4 \left(\frac{\Delta f_{mn}}{f_{mn}} \right) - 2 \left(\frac{\Delta q_0}{q_0} \right), \quad (39)$$

$$\text{or, } \frac{m' (= m + \Delta m)}{m} = 1 + 4 \left(\frac{\Delta f_{mn}}{f_{mn}} \right) - 2 \left(\frac{\Delta q_0}{q_0} \right) \quad (40)$$

Now at the time of occurrence of the first heart sound (FHS), the differential pressure or loading (q_0) across the mitral valve is very small. Hence the change in pressure loading valve (Δq_0), over the period of time of patient-tracking, will also be small compared to Δf_{mv} , and hence can be neglected in equation (40).

Hence from Eq. (39), we can compute

$$\frac{\Delta m}{m} = \left(\frac{4\Delta f_m}{f_m} \right) \quad (41)$$

to represent the change (Δm) in the parameter (m), by merely monitoring the change in frequency (Δf_{mv}) with respect to its earlier value (f_{mv}).

9. Noninvasive determination of bone osteoporosis index (in terms of bone flexural stiffness) for osteoporosis detection

Osteoporosis is a metabolic bone disease that is characterised by decreased bone mineral content and associated decreased in its mechanical strength. Thus, the osteoporotic bone is more prone to fracture.

Noninvasive measurement methods for osteoporosis detection include single and dual beam photon absorptiometry and a comparatively low cost low-frequency mechanical vibration (resonance and impedance) method [1, 12]. The low-frequency impedance response curve of (the first bending mode of) ulna yields the resonant frequency (f_r) value, which can be formulated in terms of the mechanical properties of the ulna bone, namely its bending stiffness (EI) and mass (M). It has been found that the difference between normal and osteoporotic bone is 20% in resonant frequency (f_r) and 80% in bending stiffness EI [13]. This is because f_r is the ratio of bone stiffness (EI) to mass (M), and in the pathologic osteoporotic condition both stiffness and mass decrease. Also, it has been shown that in fresh canine bone, the bending moment causing fracture has a correlation with EI of $r=0.96$ and with bone mineral content of $r=0.90$. Thus based on these results it appears that the ulna bending stiffness EI is a good indicator of bone fracture strength, which is diminished in osteoporosis. Now, both EI and M are contained in the expression for the natural frequency (f_r) of ulna vibrations, which in turn can be obtain from its resonance frequency [14]. In order to determine the resonance frequency of the ulna bone, it can be simply supported at its extremities and a vibrating probe pressed against the skin at the center of the forearm (as carried out by Steel and Gordon [14] and schematised in Fig. 8). The resonance frequency f_r (= natural frequency f_n of vibration of ulna) is obtained from the recording of the acceleration response as a function of the frequency.

If the bone is vibrating at an angular frequency p , the weight of the ulna bone per unit length is w radius of the ulna is R , and its length is ℓ , then the natural frequency f_n of the vibrating ulna beam, with its mass concentrated in the middle is given by :

$$f_n = p / 2\pi = \sqrt{(g / \delta_{st})} / 2\pi \quad (42)$$

where δ_{st} , the maximum central deflection of the simply supported ulna bone, is given by

$$\delta_{st} = w\ell^4 / (77EI) \quad (43)$$

wherein w is the ulna weight per unit length.

Hence, from (42) and (43), we get

$$f_n = \frac{1}{2\pi} \left(\frac{77gEI}{w\ell^4} \right)^{1/2} \quad (44)$$

By putting $w = \rho Ag$ ρ : bone density, A : cross-sectional area, we get

$$f_n = \frac{1}{2\pi} \left(\frac{77EI}{\rho A\ell^4} \right)^{1/2} = 1.4 \left(\frac{EI}{M\ell^3} \right)^{1/2}, \quad (45)$$

where M is the mass of the ulna bone.

By altering the frequency of the vibrating probe, we set the ulna into resonance, and the resonance frequency will be equal to the natural frequency. For f_r resonance frequency = $f_n = 400\text{Hz}$, $A = 50 \times 10^{-4}\text{m}^2$, $I = 3 \times 10^{-8}\text{m}^4$, length (ℓ) = 0.17m , $\rho = 1.8 \times 10^3 \text{ kg/m}^3$, we get $E = 20 \times 10^9 \text{ N/m}^2$ and $EI = 30\text{Nm}^2$.

Thus, from equation (45), by modeling the ulna bone as a simply-supported vibrating beam, and determining its natural transverse-vibrational frequency (equal to its measured resonance frequency f_r), we can measure its flexural stiffness EI , to detect osteoporosis.

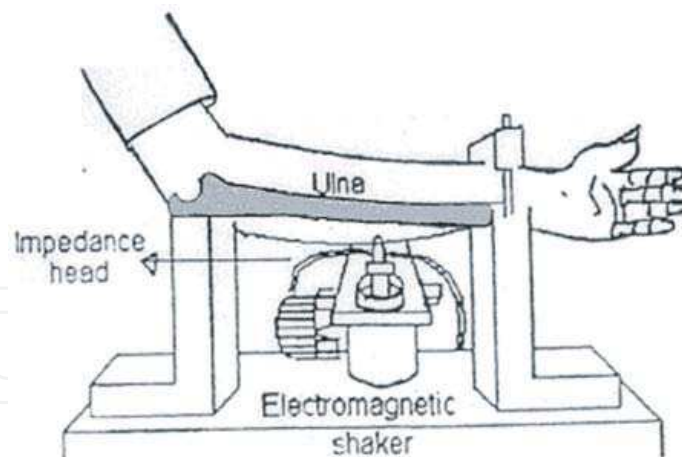


Fig. 8. Set-up used by Steel and Gordon [14] to determine the impedance of ulna. In this set up, the impedance head is attached to the moving element in the shaker. The probe, which contracts the skin, is attached to the impedance head.

10. Cardiac assessment based on Myocardial infarct detection and Intra-ventricular flow and pressure determination

In cardiology, a primary disorder is that of a heart with infarcted myocardium. This infarcted myocardial wall mitigates adequate contraction of the wall. So, the end-result of an

infarcted left ventricle (LV) is poor intra-LV velocity distribution and pressure-gradient distribution, causing impaired outflow from the LV into the aorta.

In the infarcted myocardial segments, the myocardial infrastructure of actin and myosin filaments (and their cross - bridges) is disrupted, and hence there is no contraction within these infarcted myocardial segments. Figure 9 [15] illustrates a myocardial sarcomere segment's bioengineering model, composed of two symmetrical myocardial structural units (MSUs). In these MSU(s), the contractile elements represent the actin-myosin contractile components of the sarcomere segment.

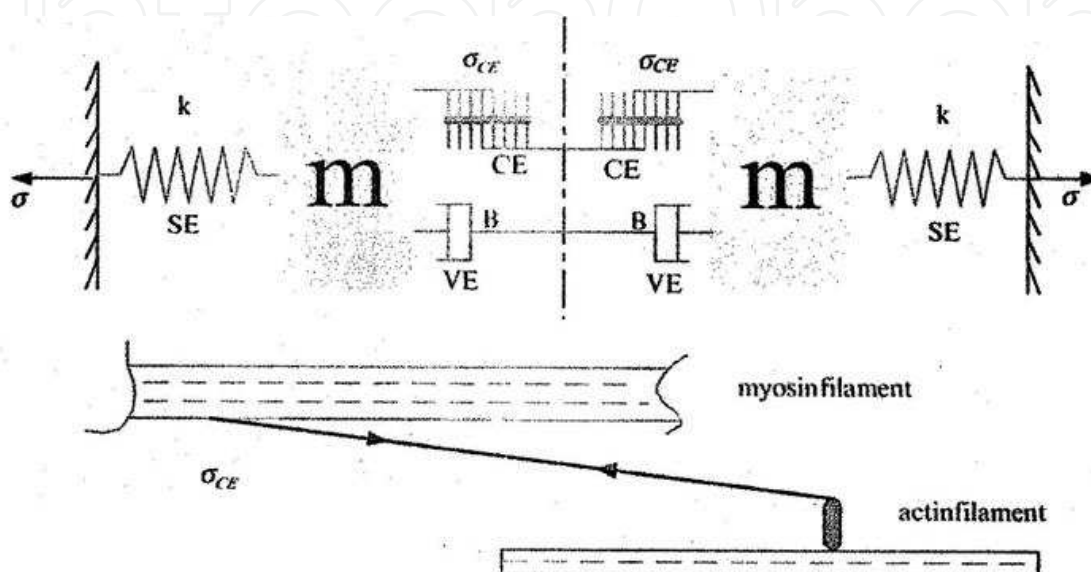


Fig. 9. Based on the conventional Hill three-element model and Huxley cross bridge theory, we have developed a myocardial model involving the LV myocardial mass, series-elastic element (SE). In this figure we have linked the anatomical associations of these myocardial model elements with microscopic structure of the heart muscle. This figure illustrates the sarcomere element contractile model, involving: the effective mass (m) of the muscle tissue that is accelerated; elastic parameter k of the series element stress σ_{SE} (k = elastic modulus of the sarcomere) viscous damping parameter B of the stress σ_{VE} in the parallel viscous element VE, the generated contractile stress σ_{CE} between myosin (thick) and actin (thin) filaments.

The disruptions of these contractile elements impairs the contractile capability of that sarcomere segment. Hence, a LV with infarcted myocardial segments will have diminished contractility, inadequate and improper intra-LV flow, and poor ejection.

Detection of myocardial infarcted segments: Now, infarcted myocardial segments can be detected as highly reflectile echo zones (HREZs) in 2- dimensional B-scan echocardiograms. In this context, we have shown earlier [16] how infarcted myocardial segments can be detected (in shape and size), by echo-texture analysis, as highly reflectile echo zones or HREZs. Now, each tissue component of the heart generates a grey scale pattern or texture related to the tissue density and fibrous content, and hence tissue stiffness.

In diseased states (such as myocardial ischemia, myocardial fibrosis, and infiltrative diseases), changes in myocardial tissue stiffness have been recognised by employing echo intensity and mean grey level of pixel as the basis for recognition of such myocardial disorders. It was found that hyper- reflectile echoes (HREs) correlated well with diseased cardiac muscle, and that myocardial tissue containing HREs corresponded with foci of sub endocardial necrosis and even calcification.

In our earlier study [15], in order to determine highly reflectile echo zones (HREZs), echocardiograms were recorded; each image was made up of 256 x 256 pixels, with each pixel having a resolution of 0-256 grey scales. The echocardiographic images were digitised into 256 grey scales. Then, echo intensity levels from normal infants were used to delineate the range of echo intensities for normal tissues. The upper bound of the echo intensity was set to 100 per cent in each normal infant, and the intensities from the rest of the image was referenced to this level. Normally, pericardium had the highest intensity level. It was found that the upper-bound of the echo intensity value for healthy tissue (expressed as a percentage of the pericardial echo intensity value) was 54.2.

Patient (Sex)	Region A	Region B	Region C	Region D	HRE and its location
B (M)	M: 167.44	54.76	51.02	82.20	105.74
	SD: 25.00	28.2	17.71	24.68	30.88
	N: 65	84	75	31	65
	P: 100	32.7	30.5	49.1	63.1
					Septum
P (F)	148.76	61.73	79.81	61.7	108.18
	26.78	23.02	22.05	24.2	13.03
	50	75	47	49	40
	100	41.5	53.8	41.5	72.6
					Septum
Br (M)	141.65	68.3	69.3	33.93	89.412
	29.56	26.8	24.8	24.4	28.0
	40	40	49	44	79
	100	41.5	53.8	41.5	73.1
					Septum
F (F)	157.34	50.1	60.8	53.8	112.1
	30.0	29.5	18.8	22.7	10.3
	35	45	49	44	31
	100	31.8	38.6	34.2	71.2
					R. ventricle
HI (M)	168.1	54.7	58.2	62.4	96.4
	21.35	21.8	16.9	20.0	14.7
	47	36	35	37	49
	100	32.5	34.6	37.1	57.3
					L. ventricle
G (M)	117.7	46.9	45.5	42.7	85.3
	20.6	19.0	20.6	19.1	22.6
	45	44	40	49	37
	100	39.8	38.7	36.2	72.5
					R. ventricle

A = Posterior Pericardium, B = Anterior Myocardium, C = Posterior Myocardium, D = Septum

Table 1. Echo intensity values for various anatomic regions of diseased pediatric hearts (based on long axis view). The numbers in the four rows represent Mean (M), Standard Deviation (SD), Number of Pixels (N), Percentage of Posterior Pericardial Intensity (P).

For patients whose echo-texture analysis showed presence of HREs, it was found that the echocardiographic intensities of the HREs from these patients intensities), were distinctly higher than the echo intensity range of normal tissue (as depicted in Table 1).

Figure 10(a) depicts an echo image of an infant with visible scars regions 1 and 2, while figures 10(b) depict printouts of the echo intensities from these two regions, wherein the infarcted segments are depicted in dark colour.

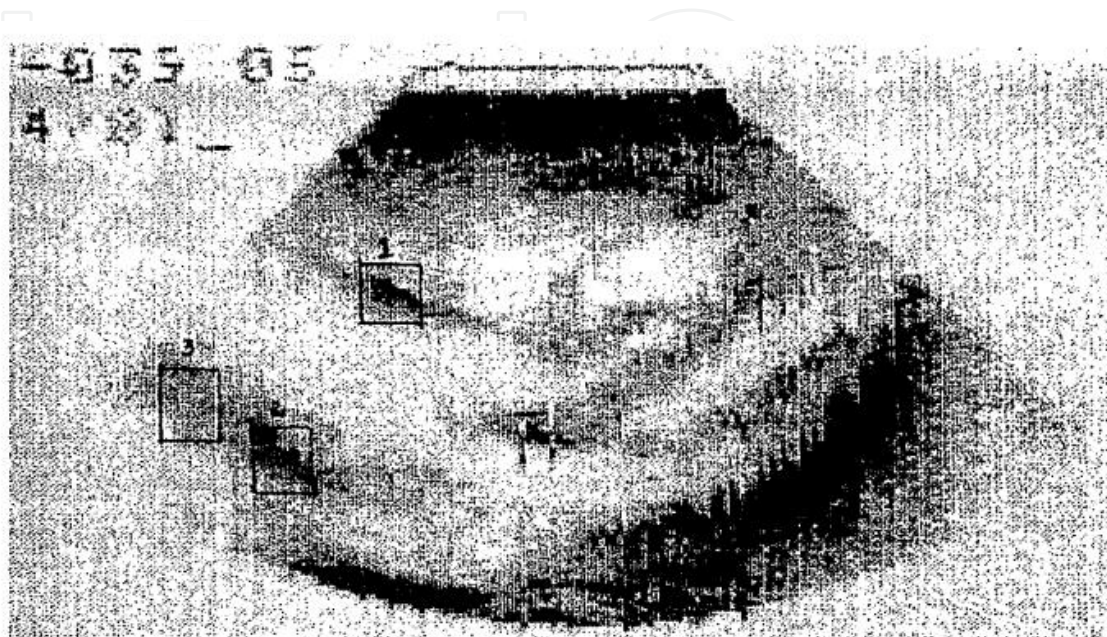


Fig. 10. (a) Long axis view of a pediatric patient's heart showing HRE regions 1 and 2 and a healthy region 3.(Adopted from the author's paper Ref 16).

Y/X	99	100	101	102	103	104	105	106	107	108	109	110	111	112	113	114
98	79	78	88	90	99	96	102	108	91	77	92	86	135	122	73	55
99	114	115	101	114	126	128	114	116	119	126	82	68	84	103	78	57
100	151	137	125	128	136	135	133	134	149	137	91	75	74	73	82	83
101	175	177	171	151	144	143	154	147	138	142	139	139	126	64	76	71
102	202	196	174	125	192	193	183	164	131	131	125	132	92	89	81	116
103	139	143	183	193	206	217	233	248	209	146	116	102	111	113	117	116
104	147	136	143	178	203	251	250	255	229	201	75	71	92	82	88	95
105	108	110	132	151	210	223	227	249	255	255	230	210	104	87	81	112
106	84	104	88	121	147	184	227	239	255	255	252	247	220	125	76	70
107	83	110	108	122	135	175	194	183	206	228	211	255	255	184	141	131
108	68	92	122	131	145	147	149	151	217	181	189	222	241	178	190	167
109	56	76	81	122	132	137	145	143	154	150	156	156	195	190	206	190
110	76	63	96	96	82	83	103	120	142	128	133	141	153	181	192	194
111	59	57	63	66	70	103	106	118	96	94	86	110	129	150	96	66
112	58	60	59	57	58	61	71	77	106	89	91	92	100	147	97	85
113	74	71	78	60	56	58	57	62	71	70	79	83	78	92	67	76
114	57	57	65	63	57	56	63	56	51	56	58	80	85	78	67	55
115	51	60	63	63	58	67	56	57	54	59	57	58	59	76	68	81

Fig. 10. (b) Pixel values corresponding to highly reflectile echo region 1. The central region having echo-intensity values greater than 200 is infarcted. (Adopted from the author's paper, Ref 16).

Myocardial tissue pixels having echo-intensity values greater than 200 were designated to be infarcted. This infarcted sub-region is seen to be surrounded by an ischemic sub-region whose pixels have echo intensity values between 100 and 200. The surrounding healthy tissue has echo intensity less than 100.

In this way, in each highly reflectile echo zone (HREZ) made up of, say, N number of pixels, we can determine the number (I) of infarcted pixels. The ration I/N represents the infarcted portion of that HREZ myocardial segment. The total number of all the infarcted pixels in all the HREZs provides an indication of the amount of infarcted myocardium of the heart or of the LV.

Intra-LV Blood Flow velocity and pressure distribution: Now, let us come to the outcome of an infarcted heart and LV. Figure 11 illustrates this outcome in the form of intra-LV blood-flow velocity and pressure (or pressure-gradient) distributions [17]. During LV diastole, from the monitored entrance velocity of blood at the mitral valve and the wall motion of the expanding LV, we can compute the intra-LV blood-flow velocity and pressure distributions, by computational fluid dynamics (CFD). During systole, from the monitored exit velocity or the aortic valve and the wall motion of the contracting LV, we can compute the intra-LV blood-flow velocity and pressure distribution by CFD.

Figure 11 illustrates the computed intra-LV blood-flow velocity and pressure distribution of a patient with an infarcted myocardium, before and after administration of nitroglycerin to determine the viability of the myocardial wall following bypass surgery. Referring to Fig 11, for the patient (with a myocardial infarct), Figs. 11(a1) depict super-imposed LV outlines at known equal intervals during diastole and systole before nitroglycerin administration, and Figs 11 (a2) depict super-imposed LV outlines at known equal intervals during diastole and systole after nitroglycerin administration; nitroglycerin is a myocardial perfusing agent, and hence a quasi-simulator of coronary bypass surgery or coronary angioplasty. From these images, we can determine the instantaneous wall displacements and hence the wall velocities at these time instants.

This data, along with the monitored entrance and exit velocities of blood into and from the LV, constitutes the data for our CFD analysis. For computational purposes, the intra-LV flow is determined from the boundary condition of LV wall-motion velocity and inlet/outlet blood flow velocity to the standard potential-flow equation $\nabla^2\Phi = 0$. The intra-LV pressure gradient can then be computed from the Bernoulli equation for unsteady potential flow.

Figures 11(b1) and 11 (c1) depict intra-LV blood-flow velocity distributions during diastole and systole, before nitroglycerin administrations.

Figures 11(b2) and 11 (c2) depict intra-LV blood-flow velocity distributions during diastole and systole, after nitroglycerin administrations

Figures 11(d1) and 11 (e1) depict intra-LV pressure distributions during diastole and systole, before nitroglycerin administrations

Figures 11(d2) and 11 (e2) depict intra-LV pressure distributions during diastole and systole, after nitroglycerin administrations

In this patient, the poor motion of the infarcted LV wall offers resistance to proper filling of the LV (Fig 11-b1). However, it can be noted that following the administration of nitroglycerin, there is improved filling of the LV (Fig. 11-b2). During systolic ejection phase, the infarcted LV wall segments do not contract, and this results in inadequate intra-LV flow velocity distribution, which mitigates adequate emptying of the LV (Fig 11-c1). Following nitroglycerin administration, there is improved outflow velocity distribution. Likewise, figures (11-d1 and 11-e1) demonstrate adverse intra-LV pressure gradients during filling and ejection phases, which are improved after administration of nitroglycerin (Eq 11-d2 and 11-e2). This has provided the basis for advocating coronary revascularization by coronary bypass surgery, for this patient.

The computed intra-LV blood-flow velocity and pressure distributions provide illustrative and quantitative outcome of an infarcted LV to the physician, which enables more distinct assessment of LV dysfunction. The cause of this LV dysfunction is provided by the echo-texture analysis of 2-d B-scan echocardiograms of HREZ(s), in terms of the amount (or number of echocardiogram image pixels) of the infarcted myocardial wall. Together, these two methodologies provide reliable and quantitative assessment of (i) how much of the LV myocardium is infarcted and its effect on the intra-LV blood flow and pressure-gradient, and (ii) intra-LV distributions of blood-flow velocity and pressure distributions, to assess candidacy for coronary bypass surgery.

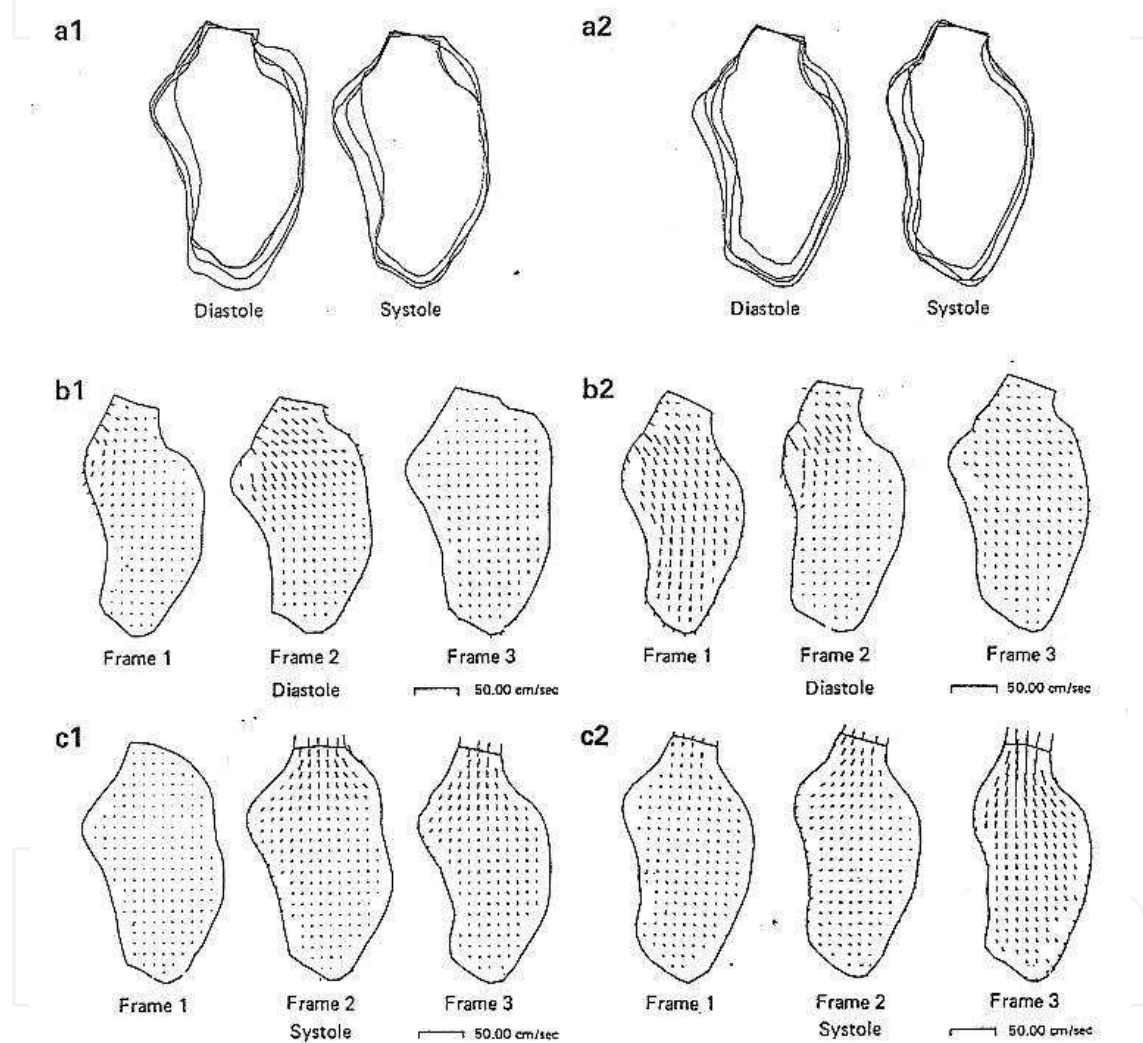


Fig. 11. (a,b,c) Patient TURN: (a) Superimposed sequential diastolic and systolic endocardial frames (whose aortic valves centres and the long axis are matched) before (1) and after (2) administration of nitroglycerin. (b) Instantaneous intra-LV distributions of velocity during diastole, before (1) and after (2) administration of nitroglycerin. (c) Instantaneous LV distributions of velocity during ejection phase, before (1) and after (2) administration of nitroglycerin. (d) Instantaneous intra-LV distributions of pressure-differentials during diastole, before (1) and after (2) administration of nitroglycerin. (e) Instantaneous intra-LV distributions (pressure-differential) during ejection phase, before (1) and after (2) administration of nitroglycerin.

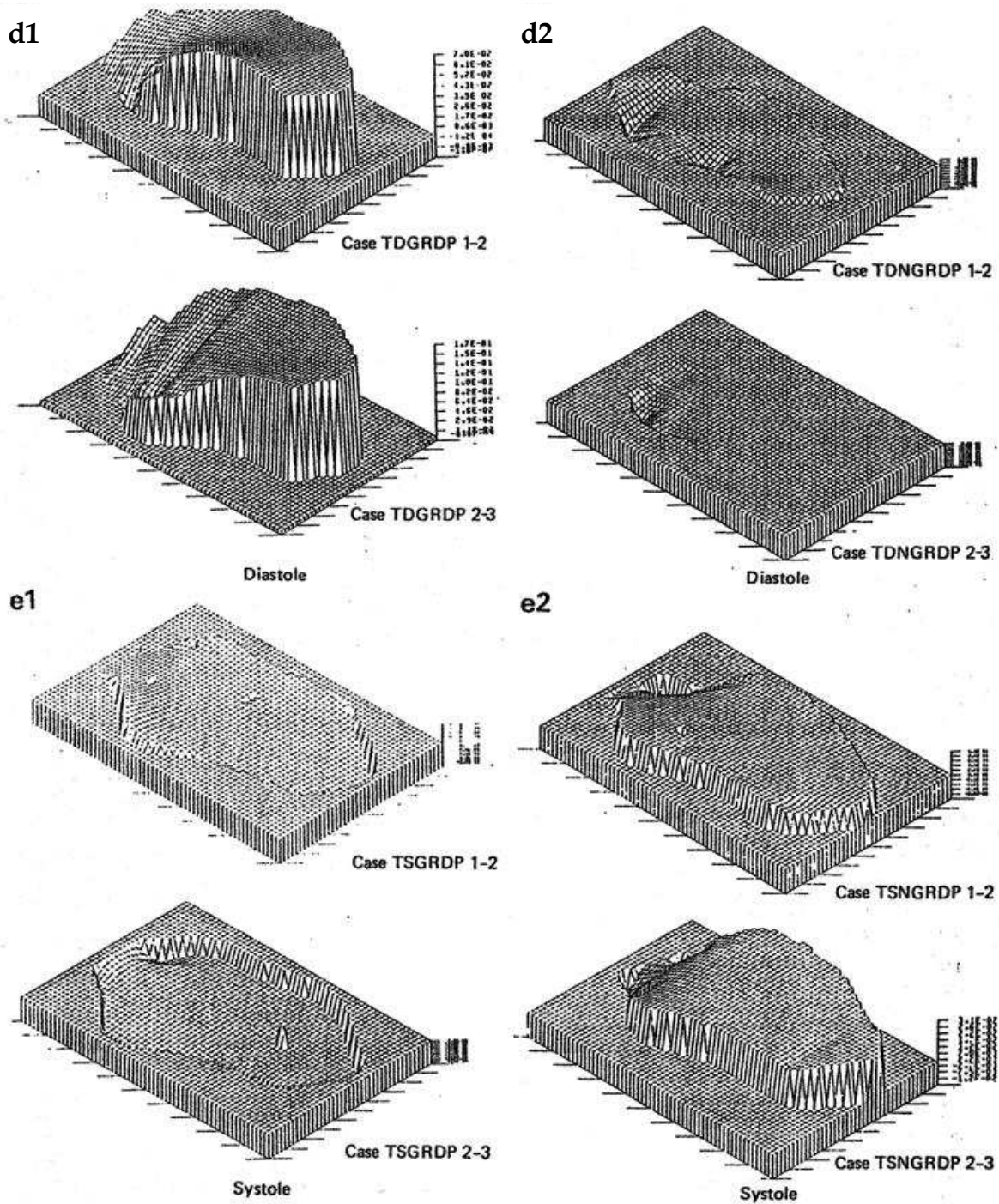


Fig. 11. (d,e) Patient TURN: (a) Superimposed sequential diastolic and systolic endocardial frames (whose aortic valves centres and the long axis are matched) before (1) and after (2) administration of nitroglycerin. (b) Instantaneous intra-LV distributions of velocity during diastole, before (1) and after (2) administration of nitroglycerin. (c) Instantaneous LV distributions of velocity during ejection phase, before (1) and after (2) administration of nitroglycerin. (d) Instantaneous intra-LV distributions of pressure-differentials during diastole, before (1) and after (2) administration of nitroglycerin. (e) Instantaneous intra-LV distributions (pressure-differential) during ejection phase, before (1) and after (2) administration of nitroglycerin.

11. Biomedical engineering concept of Heart Failure

Heart Failure, in biomedical engineering (BME) terms, can imply failure of the heart to:

- i. develop adequate contractility, due to a sizable amount of non-contractile infarcted myocardium (systolic heart failure)
- ii. generate appropriate intra-LV pressure gradient during the ejection phase, to produce adequate LV outflow rate, stroke volume and cardiac output;
- iii. produce adequate pressure increase during isovolumic contraction and ejection phases, to overcome the aortic systolic pressure;
- iv. effect adequate stroke volume, due to poor contractility (systolic heart failure) or poor filling due to diseased and stiff myocardium (diastolic heart failure).

So the factors causing systolic heart failure may be summarized to be:

1. excessive percentage amount of infarcted myocardium *PMI* (as determined by the procedure in section 10),
2. resulting incapacity of the LV to produce appropriate intra-LV pressure gradient, for adequate LV outflow velocity and flow rate dV/dt (as determined by the methodology in section 10), as manifested by the contractility index *CCI* (formulated in section 2).

Now the resultant dV/dt factor in item 2 is incorporated in the formula for *CCI* (equation 3). No doubt, the *PMI* affects *CCI*, but there is no direct formulation connecting these two indices. So we can state that *PMI* and *CCI* are the two parameters that can be attributed to the occurrence of heart failure.

We can then define the Systolic Heart Failure index, as

$$HFIN = PMI(\text{in } \%) \times HR(\text{in } s^{-1}) / CCI(\text{in } s^{-1}) \quad (46)$$

Now, in order to assess the terminal value of *HFIN*, we need to determine the terminal values of *PMI*, *CCI*, and *HR*, by studying normal subjects (as these indices are noninvasively determinable) as well as patients in different stages of heart failure.

Now, based on our studies (in Refs 4 & 5), let us (for the time being) adopt (i) the minimum acceptable value of *CCI* to be $3 s^{-1}$, (ii) the maximum acceptable value of *PMI* to be 15 %, and (iii) the maximum resting *HR* to be 120/min or $2 s^{-1}$. Substituting these values into equation (46) gives the terminal value of *HFIN* to be 10. In other words, if the value of *HFIN* exceeds the value 10, we can designate the patient to be in heart failure.

12. Concluding remarks

In this chapter, we have developed and presented noninvasive medical tests methodologies and associated NDPI(s), to make the case for reliable medical assessment of organ performance, physiological system function and dysfunction, anatomical structural property and pathology. The following tests and associated NDPI(s) have been presented:

3. Determination of cardiac contractility, from measurement of LV chamber volume and myocardial volume, in terms of the cardiac contractility index *CCI* of $(d\sigma^*/dt)_{max}$, given by equation (3).
4. Treadmill test to assess cardiac fitness and heart function, by means of the cardiac fitness index *CFI*, given by equation (8).

5. Lung Ventilation test, by monitoring lung volume by spirometry, for assessing lung ventilation and diagnosing lung disorders by means of lung ventilation index $LVPI-2$ (equation 12).
6. Oral Glucose Tolerance test, to more reliably diagnose diabetes, by determining the diabetes index DBI , given by equation (16).
7. Noninvasive determination of arterial stiffness to detect arteriosclerosis, by ultrasound measurement of arterial dimensions and pulse wave velocity and auscultatory diastolic pressure, by means of the arteriosclerosis index $ART-NPI$, given by equation (20).
8. Noninvasive determination of (i) Aortic Pressure profile and (ii) Aortic normal vs disease state property in terms of the *Aortic number* given by equation (31), by monitoring the left ventricular outflow into the aorta and auscultatory diastolic and systolic pressures.
9. Noninvasive determination of Mitral valve pathology, by (i) monitoring its vibrational frequency from the first heart sound spectrum, and its size parameter from 2-d echocardiogram, and (ii) employing this data to structure its E^* vs. σ^* constitutive property (equations 36 and 37), and determine the alteration in the value of the constitutive index m given by equation (40).
10. Characterization of Osteoporosis, by determining the ulna bone vibratory resonance frequency, in terms of its flexural stiffness EI , given by equation (45).
11. Quantitative determination of (i) the amount of infarcted myocardial segment of the heart from echo-texture analysis of 2-d echo cardiograms (figure 10), and (ii) associated outcome of LV dysfunction in terms of the intra-LV blood-flow velocity and pressure distributions (figure 11).

Together these tests and their associated NDPI (s) can provide more reliable medical assessment. What now needs to be done is (i) application of these tests to large patient populations, and (ii) determination of the ranges of NDPI (s) for normal and abnormal states of organs, physiological systems and anatomical structures.

All of these tests can be employed in tertiary patient case, through the department of biomedical engineering (BME) in a tertiary-care medical center. This makes a strong case for the institution of BME departments in tertiary care medical centers, which will revolution therapy health care.

13. References

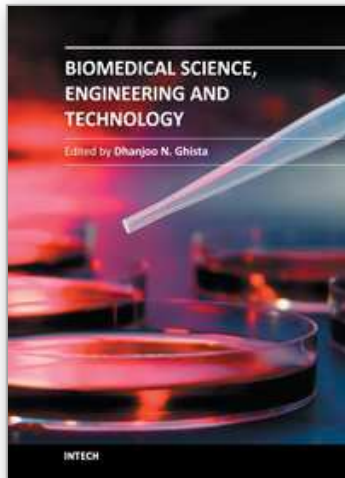
- [1] "Physiological Systems' Numbers in Medical Diagnosis and Hospital Cost-effective Operation", by Dhanjoo N. Ghista, in *Journal of Mechanics in Medicine & Biology* 2005, vol 4, No.4.
- [2] *Applied Biomedical Engineering Mechanics*, by Dhanjoo N. Ghista, CRC press (Taylor & Francis Group) Baton Rouge Florida 334872-2742, ISBN 978-0-8247-5831-8, 2008
- [3] Measures and indices of intrinsic characterization of cardiac dysfunction during filling & systolic ejection," by Liang Zhong, Dhanjoo N. Ghista, Eddie Y-K. Ng, Lim SooTeik and Chua Siang Jin, in *Journal of Mechanics in Medicine & Biology* 2005, 5(2):37-322.

- [4] "Validation of a novel noninvasive characterization of cardiac index of left ventricle contractility in patients", by Zhong L, Tan RS, Ghista DN, Ng E. Y-K, Chua LP, Kassab GS, *Am J Physiol Heart CircPhysiol*2007, 292:H2764-2772.
- [5] "Effects of Surgical Ventricular Restoration on LV Contractility assessed by a novel Contractility index in patients with Ischemic cardiomyopathy", by Zhong L, Sola S, Tan RS, Le TT, Ghista DN, Kurra V, Navia JL, Kassab G.; in *Am J Cardiology*, 2009;103(5):674-679.
- [6] Cardiac Fitness mathematical Model of Heart-rate response to V02 during and after Stress-Testing", Lim GeokHian, Dhanjoo N. Ghista, Koo TseYoong, John Tan Cher Chat, Philip EngTiew& Loo Chian Min; *International Journal of Computer Application in Technology(Biomedical Engineering & Computing Special Issue)*, Vol 21, No 1/2, 2004.
- [7] "Glucose Tolerance Test Modeling & Patient-Simulation for Diagnosis", by Sarma Dittakavi & Dhanjoo N. Ghista, *Journal of Mechanics in Medicine & Biology*, Vol. 1, No.2, Oct.2001.
- [8] "Determination of the In-vivo Elasticity of Blood Vessel and Detection of Arterial Disease", by D. N. Ghista, *Automedica*, Vol. 1, No. 3, 1974.
- [9] "Determination of Aortic Pressure-time Profile , Along with Aortic Stiffness and Peripheral Resistance", by Liang Zhong, Dhanjoo N. Ghista, Eddie Y-K. Ng, Lim SooTeik and Chua Siang Jin, in *Journal of Mechanics in Medicine & Biology* 2004, 4(4):499-509.
- [10] "Mechanics of the Mitral Valve: Stresses in the Membrane, Indirect Determination of the Instantaneous Modulus of the Membrane", by D.N. Ghista; *Journal of Biomechanis*, Vol. 5, No. 3, 1972.
- [11]"Mitral Valve Mechanics - Stress/Strain Characteristics of Excise Leaflets, Analysis of its Functional Mechanics and its Medical Applications", by D. N. Ghista and A. P. Rao: *Medical and Biological Engineering*, Vol. 11, No. 6, 1973.
- [12] In Vivo Measurement of the Dynamic Response of Bone, by J.M. Jurist, H.D. Hoeks, D.A. Blackketter, R. K. Snyder and E.R. Gardner, in *Orthopaedic Mechanics: Procedures and Devices (Volume III)*,ed by Dhanjoo N. Ghista and Robert Roaf, Academic Press (London), 1981.
- [13] Noninvasive determination of Ulna stiffness from Mechanical Response---In Vivo comparison of stiffness and Bone mineral content in humans, by C.R. Steele, L.J. Zhou, D.Guido, R. Marcus, W. L. Heinrichs and C. Cheema, in *Journal of Biomechanical Engineering*, Vol. 10 (87), 1988.
- [14] Preliminary Clinical results using SOBSA for noninvasive determination of ulna bending stiffness, by C.R. Steele and A.F. Gordon, in *Advances in Bioengineering (ASME)*, edited by R. C Eberhand and A.H. Burstein, 1978, pp 85-87.
- [15] Measures and Indices for Intrinsic Characterization of Cardiac Dysfunction during Filling and Systolic Ejection, by Liang Zhong, Dhanjoo N. Ghista, Eddie Y. Ng, Lim SooTeik, and Chua Siang Jin, in *Journal of Mechanics in Medicine and Biology*,Vol 5, No. 2, 2005.

- [16] Detection of myocardial scars in neonatal infants from computerised echocardiographic texture analysis, by M.V Kamath, R.C Way, D.N. Ghista, T.M. Srinivasan, C. Wu, S Smeenk, C. Manning, J. Cannon, *Engineering in Medicine*, Vol. 15, No.3, 1986
- [17] Intrinsic Indices of the Left Ventricle as a Blood Pump in Normal and Infarcted Left Ventricle, by K. Subbaraj, D.N. Ghista, and E. L. Fallen, in *J of Biomedical Engineering*, Vol 9, July issue, 1987

IntechOpen

IntechOpen



Biomedical Science, Engineering and Technology

Edited by Prof. Dhanjoo N. Ghista

ISBN 978-953-307-471-9

Hard cover, 902 pages

Publisher InTech

Published online 20, January, 2012

Published in print edition January, 2012

This innovative book integrates the disciplines of biomedical science, biomedical engineering, biotechnology, physiological engineering, and hospital management technology. Herein, Biomedical science covers topics on disease pathways, models and treatment mechanisms, and the roles of red palm oil and phytochemical plants in reducing HIV and diabetes complications by enhancing antioxidant activity. Biomedical engineering covers topics of biomaterials (biodegradable polymers and magnetic nanomaterials), coronary stents, contact lenses, modelling of flows through tubes of varying cross-section, heart rate variability analysis of diabetic neuropathy, and EEG analysis in brain function assessment. Biotechnology covers the topics of hydrophobic interaction chromatography, protein scaffolds engineering, liposomes for construction of vaccines, induced pluripotent stem cells to fix genetic diseases by regenerative approaches, polymeric drug conjugates for improving the efficacy of anticancer drugs, and genetic modification of animals for agricultural use. Physiological engineering deals with mathematical modelling of physiological (cardiac, lung ventilation, glucose regulation) systems and formulation of indices for medical assessment (such as cardiac contractility, lung disease status, and diabetes risk). Finally, Hospital management science and technology involves the application of both biomedical engineering and industrial engineering for cost-effective operation of a hospital.

How to reference

In order to correctly reference this scholarly work, feel free to copy and paste the following:

Dhanjoo N. Ghista (2012). Physiological Nondimensional Indices in Medical Assessment: For Quantifying Physiological Systems and Analysing Medical Tests' Data, Biomedical Science, Engineering and Technology, Prof. Dhanjoo N. Ghista (Ed.), ISBN: 978-953-307-471-9, InTech, Available from:
<http://www.intechopen.com/books/biomedical-science-engineering-and-technology/physiological-nondimensional-indices-for-medical-assessment->

INTECH
open science | open minds

InTech Europe

University Campus STeP Ri
Slavka Krautzeka 83/A
51000 Rijeka, Croatia
Phone: +385 (51) 770 447
Fax: +385 (51) 686 166

InTech China

Unit 405, Office Block, Hotel Equatorial Shanghai
No.65, Yan An Road (West), Shanghai, 200040, China
中国上海市延安西路65号上海国际贵都大饭店办公楼405单元
Phone: +86-21-62489820
Fax: +86-21-62489821

www.intechopen.com

www.intechopen.com

IntechOpen

IntechOpen

© 2012 The Author(s). Licensee IntechOpen. This is an open access article distributed under the terms of the [Creative Commons Attribution 3.0 License](#), which permits unrestricted use, distribution, and reproduction in any medium, provided the original work is properly cited.

IntechOpen

IntechOpen